HAL open science

The mechanism behind internally generated centennial-to-millennial scale climate variability in an earth system model of intermediate complexity

T. Friedrich, A. Timmermann, L. Menviel, O. Elison Timm, A. Mouchet, Didier M. Roche

To cite this version:

T. Friedrich, A. Timmermann, L. Menviel, O. Elison Timm, A. Mouchet, et al.. The mechanism behind internally generated centennial-to-millennial scale climate variability in an earth system model of intermediate complexity. Geoscientific Model Development, 2010, 3 (2), pp.377-389. 10.5194/gmd-3-377-2010 . hal-03200226

HAL Id: hal-03200226

https://hal.science/hal-03200226v1

Submitted on 18 Apr 2021

HAL is a multi-disciplinary open access archive for the deposit and dissemination of scientific research documents, whether they are published or not. The documents may come from teaching and research institutions in France or abroad, or from public or private research centers.

L'archive ouverte pluridisciplinaire **HAL**, est destinée au dépôt et à la diffusion de documents scientifiques de niveau recherche, publiés ou non, émanant des établissements d'enseignement et de recherche français ou étrangers, des laboratoires publics ou privés.

Geosci. Model Dev., 3, 377–389, 2010
www.geosci-model-dev.net/3/377/2010/
doi:10.5194/gmd-3-377-2010
© Author(s) 2010. CC Attribution 3.0 License.

Geoscientific Model Development

The mechanism behind internally generated centennial-to-millennial scale climate variability in an earth system model of intermediate complexity

T. Friedrich[1], **A. Timmermann**[1], **L. Menviel**[1,*], **O. Elison Timm**[1], **A. Mouchet**[2], **and D. M. Roche**[3]

[1]IPRC, University of Hawaii, 2525 Correa Road, Honolulu, HI 96822, USA
[2]Département Astrophysique, Géophysique et Océanographie, Université de Liège, Liège, Belgium
[3]Section Climate Change and Landscape Dynamics, Department of Earth Sciences, Vrije Universiteit Amsterdam, De Boelelaan 1085, 1081 HV Amsterdam, Netherlands
[*]now at: Climate and Environmental Physics, Physics Institute, University of Bern, Bern, Switzerland

Received: 27 January 2010 – Published in Geosci. Model Dev. Discuss.: 25 February 2010
Revised: 13 July 2010 – Accepted: 22 July 2010 – Published: 25 August 2010

Abstract. The mechanism triggering centennial-to-millennial-scale variability of the Atlantic Meridional Overturning Circulation (AMOC) in the earth system model of intermediate complexity LOVECLIM is investigated. It is found that for several climate boundary conditions such as low obliquity values (∼22.1°) or LGM-albedo, internally generated centennial-to-millennial-scale variability occurs in the North Atlantic region. Stochastic excitations of the density-driven overturning circulation in the Nordic Seas can create regional sea-ice anomalies and a subsequent reorganization of the atmospheric circulation. The resulting remote atmospheric anomalies over the Hudson Bay can release freshwater pulses into the Labrador Sea and significantly increase snow fall in this region leading to a subsequent reduction of convective activity. The millennial-scale AMOC oscillations disappear if LGM bathymetry (with closed Hudson Bay) is prescribed or if freshwater pulses are suppressed artificially. Furthermore, our study documents the process of the AMOC recovery as well as the global marine and terrestrial carbon cycle response to centennial-to-millennial-scale AMOC variability.

1 Introduction

Oxygen isotope records from Greenland (Johnsen et al., 1992; Dansgaard, 1993; GRIP Project Members, 1993; NGRIP Project Members, 2004) bear witness to the existence of abrupt climate reorganizations in the Northern Hemisphere. Dansgaard-Oeschger (DO) events (Dansgaard et al., 1982; Oeschger et al., 1984), i.e. rapid transitions from stadial to interstadial conditions, are prominent features of the last glacial period. The associated temperature response referred to as the bipolar seesaw pattern (Stocker, 1998) has prompted researchers to hypothesize that their dynamics is tightly coupled to the Atlantic Meridional Overturning Circulation (AMOC) (Ganopolski and Rahmstorf, 2001; Alley et al., 2001; Timmermann et al., 2003). In simplified and intermediate complexity models (Stommel, 1961; Broecker et al., 1990; Ganopolski and Rahmstorf, 2001) the AMOC is known to be a nonlinear system with multiple equilibrium solutions and thresholds for transitions between different modes of operation. Stochastic and periodic excitation of such a bistable system can generate dynamical behaviour that resembles the observed DO events (Alley et al., 2001).

In fact, the observed DO events bear some similarity to the so-called ocean relaxation oscillations. Their mechanism involves a long "recharging" timescale, often associated with advective or diffusive processes and a rapid "flushing" process, such as oceanic convection. Internally generated centennial to millennial-scale relaxation oscillations of the AMOC have been simulated in ocean and climate models of varying complexity (Winton, 1993; Winton and Sarachik, 1993; Paul and Schulz, 2002; Timmermann and Goosse, 2004; Rial and Yang, 2007; Schulz et al., 2007; Jongma et al., 2007; Rial and Saha, 2008) and have often been explained in terms of the deep-decoupling oscillation concept (Winton, 1993). The deep-decoupling phase of such an oscillation describes a state with little North Atlantic deep-water formation (due to reduced surface densities). Under such conditions subsurface advective or diffusive heating can lead

Correspondence to: T. Friedrich
(tobiasf@hawaii.edu)

Published by Copernicus Publications on behalf of the European Geosciences Union.

Table 1. Summary of modelling studies that observed low-frequency AMOC oscillations in the ECBilt-CLIO climate model.

Model study	Background conditions and forcing	AMOC variability
Goosse et al. (2002)	pre-industrial reduction of solar constant in 3 sensitivity runs	several spontaneous transitions of ±5 Sv in all simulations
Rial and Yang (2007)	intermediate between LGM LGM and pre-industrial	several spontaneous transitions between a strong and a weak AMOC state (no values given)
Schulz et al. (2007)	pre-industrial, freshwater forcing of 5, 7.5 and 10 mSv respectively added to the precipitation over the southern Labrador Sea	bi-modal AMOC with ±3 Sv
Jongma et al. (2007)	pre-industrial, freshwater forcing of 5, 7.5 and 10 mSv respectively added to the precipitation over the southern Labrador Sea	"on" and "off" switches in Labrador Sea convection ±3 Sv AMOC changes
Rial and Saha (2008)	multiple runs ranging from LGM to pre-industrial background climate (different orbital and albedo configurations)	no oscillations for LGM and pre-industrial climate; several spontaneous AMOC transitions for intermediate boundary conditions (no values given)
this study	multiple runs with pre-industrial and intermediate climate (different orbital and albedo configurations)	no oscillations for pre-industrial climate; several spontaneous AMOC transitions (up to ±5 Sv) for intermediate climate

to a de-stabilization of the water column in the convective areas of the North Atlantic and eventually a convective flush that enhances North Atlantic Deep Water Formation and the meridional overturning circulation. Such flushes are associated with increased poleward heat transport that may provide a self-limiting negative feedback to the AMOC.

Several modelling studies aimed at analysing the mechanism triggering DO events using the ECBilt-CLIO climate model (Table 1). The findings of Schulz et al. (2007) and Jongma et al. (2007) indicate that small freshwater perturbations in the Labrador Sea can lead to a bi-stable behaviour of the AMOC under Holocene climate conditions. Jongma et al. (2007) conclude that their results give further support hypothesis on the existence of a multi-centennial scale amplifying mechanism that operates under Holocene conditions.

Using the same earth system model the studies by Rial and Yang (2007); Rial and Saha (2008) have claimed that Greenland ice-core data can be interpreted in terms of a frequency modulated relaxation oscillation. According to their hypothesis internally generated deep-decoupling oscillations in the North Atlantic become frequency modulated by orbitally-induced changes of the solar radiation.

A multi-millennia simulation by Goosse et al. (2002) exhibited abrupt climate events lasting for several centuries caused by transitions in the AMOC. Their sensitivity experiments showed that a reduction in solar irradiance can trigger the observed transitions.

Inspired by these findings, we set forth to further elucidate the physical mechanisms responsible for the generation of centennial-millennial-scale climate variability in the ECBilt-CLIO climate model. In set of experiments using different climate background conditions we can qualitatively reproduce the low-frequency AMOC oscillations described in the publications above. We will show that the underlying mechanism in the model must be fundamentally different from the one that caused DO events during the last glacial period. Irrespective of the triggering mechanism we analyse the global impact of the AMOC weakening and the mechanism that leads to its resumption.

This paper is organized as follows: after a brief description of the model and the experiments in the subsequent two sections (2 and 3), we describe the main results from a suite of climate sensitivity experiments in Sect. 4. In Sect. 5 we discuss and summarize the main implications of our findings.

2 Model configuration

We conducted a series of climate sensitivity experiments using the atmosphere-ocean-sea ice-carbon cycle model LOVECLIM (Driesschaert, 2005). LOVECLIM is based on the ECBilt-CLIO EMIC extended by vegetation and marine carbon cycle components.

Its sea ice-ocean component (CLIO) (Goosse et al., 1999) consists of a primitive equation level model with $3° \times 3°$ resolution on a partly rotated grid in the North Atlantic. CLIO uses a free surface and is coupled to a thermodynamic-dynamic sea ice model. In the vertical there are 20 unevenly spaced levels with a thickness ranging from 10 m near the surface to ∼700 m below 3000 m. Mixing along isopycnals, vertical mixing as well as the effect of mesoscale eddies

on transports and mixing and downsloping currents at the bottom of continental shelfs are parametrized. The Bering Strait is closed in our simulations which inhibits freshwater transport from the Pacific into the Arctic.

The atmosphere model (ECBilt) is a spectral T21, based on quasigeostrophic equations with 3 vertical levels and a horizontal resolution of about $5.625° \times 5.625°$. Ageostrophic forcing terms are estimated from the vertical motion field and added to the prognostic vorticity equation and thermodynamic equation. Diabatic heating due to radiative fluxes, the release of latent heat and the exchange of sensible heat with the surface are parametrized. The seasonally and spatially varying cloud cover climatology is prescribed in ECBilt.

The ocean, atmosphere and sea ice component of the ECBilt-CLIO model are coupled by exchange of momentum, heat and freshwater fluxes. The hydrological cycle over land is closed by a bucket model for soil moisture and simple river runoff scheme. Due to the weakness of the tropical trade winds simulated by the model, the moisture transport from the Atlantic to the Pacific is too weak. To generate an Atlantic salty enough for an AMOC, a small correction for freshwater flux is prescribed redirecting snow- and rainfall over the Atlantic to the North Pacific.

The terrestrial vegetation module of LOVECLIM, VECODE is described by Brovkin et al. (1997). On the basis of annual mean values of several climatic variables, the VECODE model computes the evolution of the vegetation cover described as a fractional distribution of desert, tree, and grass in each land grid cell once a year. Within the LOVECLIM version used here, simulated vegetation changes affect only the land surface albedo, and have no influence on other processes such as evapotranspiration or surface roughness.

LOCH is a 3-D global model of the oceanic carbon cycle with prognostic equations for dissolved inorganic carbon, total alkalinity, phosphate , organic products, oxygen and silicates (Mouchet and Francois, 1996). LOCH is coupled to CLIO, using the same time step. Biogeochemical tracers in LOCH are advected with the CLIO circulation field and are subject to horizontal and vertical mixing. The phytoplankton growth depends on the availability of nutrients (phosphate) and light, with a weak temperature dependence. A grazing process together with natural mortality limit the primary production and provide the source term for the organic matter sinking to depth. The atmospheric CO_2 content is predicted for each ocean time step from the air-sea CO_2 fluxes calculated by LOCH as well as from the air-terrestrial biomass CO_2 fluxes provided by VECODE.

A more detailed description of the LOVECLIM model together with an evaluation of its performance under present-day and LGM climate can be found in Menviel et al. (2008).

Table 2. Acronym, obliquity, albedo and bathymetry for different model runs. For all runs eccentricity, precession, sea level, land topography and atmospheric CO_2 concentration were kept at pre-industrial values.

Model run	Obliquity	Albedo	Bathymetry
CTR	23.446°	present-day	present-day
LGMALB	23.446°	"flat" LGM ice sheet	present-day
OBL22.4	22.4°	present-day	present-day
OBL22.1	22.1°	present-day	present-day
COMBI	22.1°	"flat" LGM ice sheet	present-day
LGM22.1	22.1°	present-day	LGM

3 Experiments

A set of experiments was conducted to study the parameters settings under which the model exhibits internally-generated low-frequency variability of the AMOC as well as the triggering mechanism (Table 2). A pre-industrial baseline simulation was obtained with LOVECLIM by first prescribing present-day orbital parameters, bathymetry, land albedo and topography and by forcing the model with an atmospheric CO_2 concentration of 287 ppmv for 500 years. Thereafter by activating the coupling between the carbon cycle and the climate components, the atmospheric CO_2 concentrations are allowed to vary freely for another 1700 years. The mean climate of the baseline run was described in Menviel et al. (2008). A new control run (CTR, in Table 2) was integrated from this equilibrium for 8000 years. Subsequently, several model runs were conducted for at least 5000 years using different values for obliquity and northern-hemispheric albedo respectively while keeping pre-industrial values for all other boundary conditions (see Table 2). In addition, a 2000 year-long sensitivity run was performed with LOVECLIM using LGM-bathymetry values (Roche et al., 2007) and an obliquity value of 22.1°.

In the present study the model is exclusively forced by different obliquity and albedo values. No use has been made of additional constant (Schulz et al., 2007) or time-varying (Ganopolski and Rahmstorf, 2001) freshwater perturbations.

4 Results

4.1 AMOC response to different background climate

The climatological formation sites of North Atlantic Deep Water in our model are located in the eastern Greenland Iceland Norway (GIN) Sea, Labrador Sea and Irminger Sea. The meridional streamfunction of the CTR run that characterizes the Atlantic meridional overturning circulation (Fig. 1) exhibits the two main deepwater formation branches: one north and one south of the Greenland-Scotland Ridge.

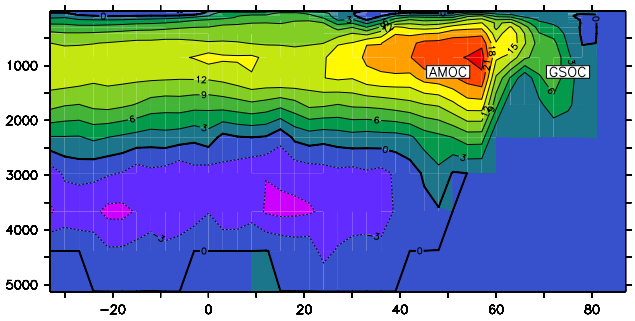

Fig. 1. Mean Atlantic Meridional Overturning Circulation for the control simulation in Sv. The two cells that are referred to in the text – GIN Sea overturning circulation (GSOC) and maximum of Atlantic overturning circulation (AMOC) – are indicated by the labels.

In the following we will refer to GIN Sea overturning circulation as "GSOC" and to the maximum of the Atlantic meridional overturning circulation (including the GIN Sea) simply as "AMOC". We define the GSOC index as the maximum value of the meridional stream function north of the Greenland-Scotland Ridge, whereas the AMOC index refers to the overall maximum of the streamfunction in the North Atlantic.

Figure 2 compares the simulated variations in the GSOC and the AMOC for the control run (CTR) and the four runs under different climate boundary conditions (LGMALB, OBL22.4, OBL22.1, COMBI). The overturning indices in the CTR run under present-day climate conditions do not exhibit any significant low-frequency variability (Fig. 2a, f). The LGMALB run is characterized by an increased GSOC variability (Fig. 2b) and an abrupt weakening "event" in both indices which lasts for about 200 years similar to results of Goosse et al. (2002). Lowering obliquity from 23.444 to 22.4 has a similar but somewhat stronger effect on the low-frequency variability (Fig. 2c, h). GSOC varies by about ±2.5 Sv and these variations are accompanied by numerous abrupt transitions between a strong AMOC state (∼26 Sv) and an intermediate state (∼19 Sv). The timescale of this variability ranges from 1000–1500 years. Further reduction of the obliquity to 22.1° (Fig. 2d, i) leads to a shift of the pause-pulse ratio: the AMOC is now preferentially operating in the intermediate regime (∼19 Sv), rather than in the strong AMOC state. Similar changes of the pause-pulse ratio of millennial-scale AMOC variability can be induced by external freshwater forcing, as described in the idealized box-modelling study of Schulz et al. (2002) and the LOVECLIM modelling study of Schulz et al. (2007) and Jongma et al. (2007). For a combination of low obliquity and a LGM-albedo (COMBI run) abrupt transitions appear to be less frequent and the intermediate regime is characterized by higher AMOC values (∼23 Sv).

4.2 Mechanism of centennial-to-millennial-scale AMOC variability

To elucidate the physical mechanisms responsible for the generation of centennial-to-millennial-scale GSOC and AMOC variability, we focus on only one event in the OBL22.4 run (model years 2450–3050). Further statistical analysis (not shown) revealed that the same mechanism operates in the other experiments and for other individual events.

Figure 3b–g documents crucial stages during an AMOC cycle in the OBL22.4 experiment as well as the associated states of the two overturning cells (Fig. 3a). In our simulation an event is initiated by a random reduction of the GSOC. This reduction leads to a decrease of meridional heat transport into the GIN Sea and an associated decline in SST in the sinking region of ∼2–5 K (not shown). The drop in SST causes an increase in sea ice coverage in the considered region (not shown). The position of the sea ice (defined here as the position of the 0.1 m sea ice thickness contour) shifts southward by several degrees latitude, now covering the major part of the sinking region. Sea ice insulates the ocean surface from heat loss which leads to a further reduction of the strength of the overturning (Fig. 3b). As a consequence of the sea-ice expansion, surface air temperature (SAT) decreases in the Nordic Seas by up to 20 K (Fig. 3c, shaded). The resulting geopotential height anomaly over the eastern North Atlantic exhibits a baroclinic structure in the vertical similar to the response to negative SST anomalies in Deser et al. (2004). A surface boundary layer high pressure anomaly develops over the GIN Sea that is accompanied by low pressure anomalies over southern Greenland and the Hudson Bay (Fig. 3c, contours). As we shall see later the resulting wind stress anomalies over the Hudson Bay are crucial for the reduction of Labrador Sea convection and eventually the weakening of the AMOC. Due to the model representation of river runoff, sea surface salinity (SSS) in the Hudson Bay is about 1.4 psu lower (∼33.60 psu) than in the adjacent Labrador Sea (∼34.98 psu) – in accordance with the Levitus Climatology (Levitus, 1994). Under climatological conditions the zonal salinity gradient between Hudson Bay and Labrador Sea is maintained by north-westerly winds. As a result of the altered near surface pressure pattern (Fig. 3c, contours), the meridional wind stress component near Hudson Strait is strongly reduced which results in a flush of fresher water from the Hudson Bay into the Labrador Sea (Figs. 3c, d and 4a). Moreover, the anomalous low pressure near Hudson Bay leads to a significant increase in snow fall further freshening surface waters (Fig. 4c). The resulting drop of SSS in the Labrador Sea (Fig. 3d, contours, Fig. 4c) leads to a major reduction of Labrador Sea convection and a subsequent decrease of the North Atlantic overturning circulation strength by about 8 Sv (Fig. 3a–phase d). A part of this fresh surface water is advected from the Labrador Sea into the GIN Sea, thereby maintaining the halocline in the GIN Sea. In OBL22.4 this state of reduced overturning lasts

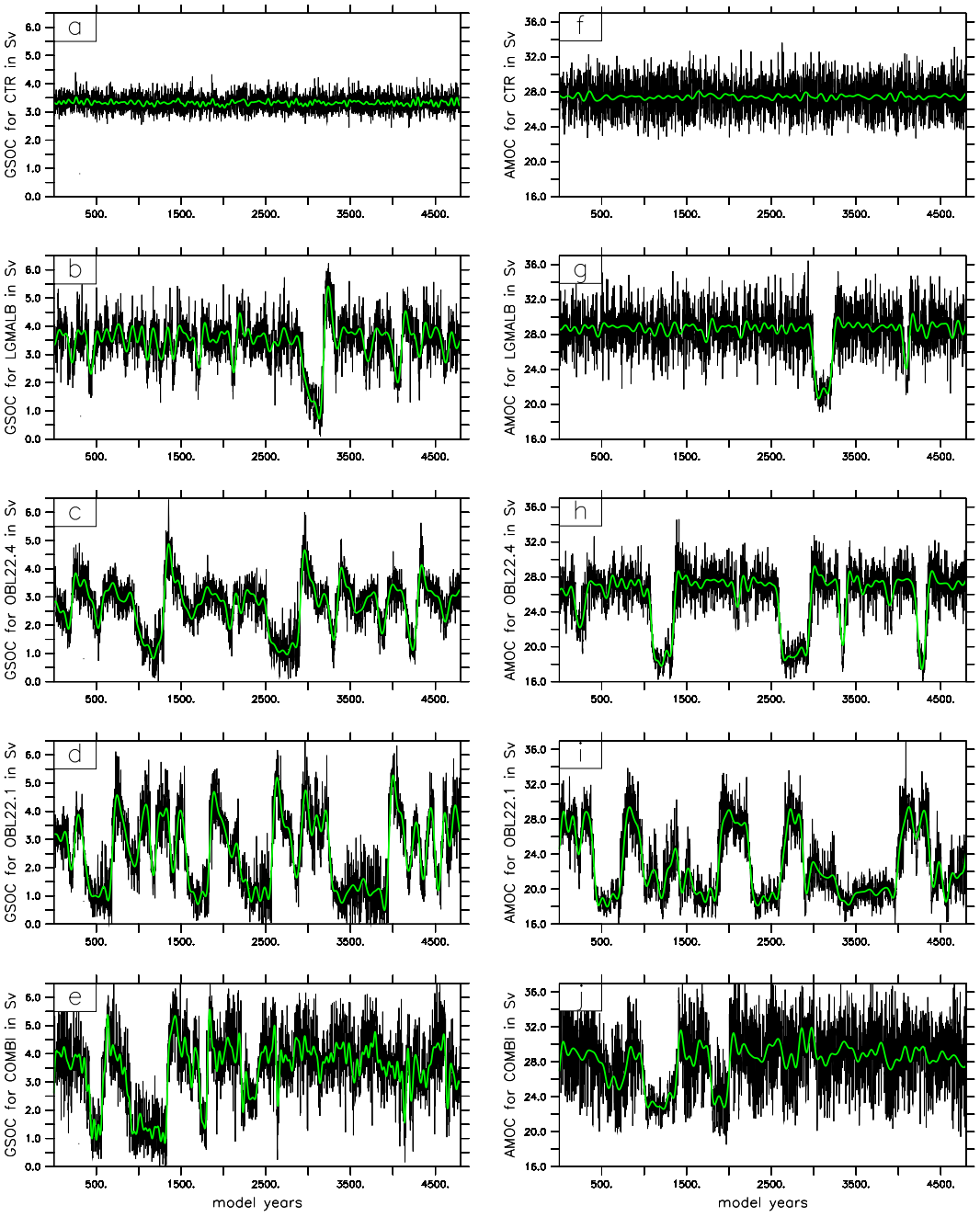

Fig. 2. GIN Sea overturning circulation (GSOC) **(a–e)** and maximum of Atlantic overturning circulation (AMOC) **(f–j)** in Sv for indicated model simulations. Please refer to Table 2 for an explanation of the simulations. A low pass filter of 50 years was applied for green lines.

for about 300 years. Anomalies in the annual mean convective layer depth (CLD) attain values of up to −200 m in the Labrador Sea and up to −400 m in the GIN Sea[1]. The atmospheric response pattern to the GIN Sea near-surface temperature anomalies is persistent throughout the entire period of AMOC weakening (Fig. 3e). The recovery phase of the AMOC (Fig. 3f, g) is associated with subsurface warming of the GIN Sea (Fig. 3f). Subsurface temperature anomalies in this region reach values of up to 4 K. Compared to the unperturbed variance of subsurface temperature variations of 0.26 K, a 4 K anomaly during the recovery phase represents an unprecedented warming of the subsurface and deep-water layers – a phenomenon known as deep decoupling. Even though GSOC is strongly reduced in phases e and f (see Fig. 3a), warm and salty water from the North Atlantic Drift

[1] In wintertime these anomalies are much larger.

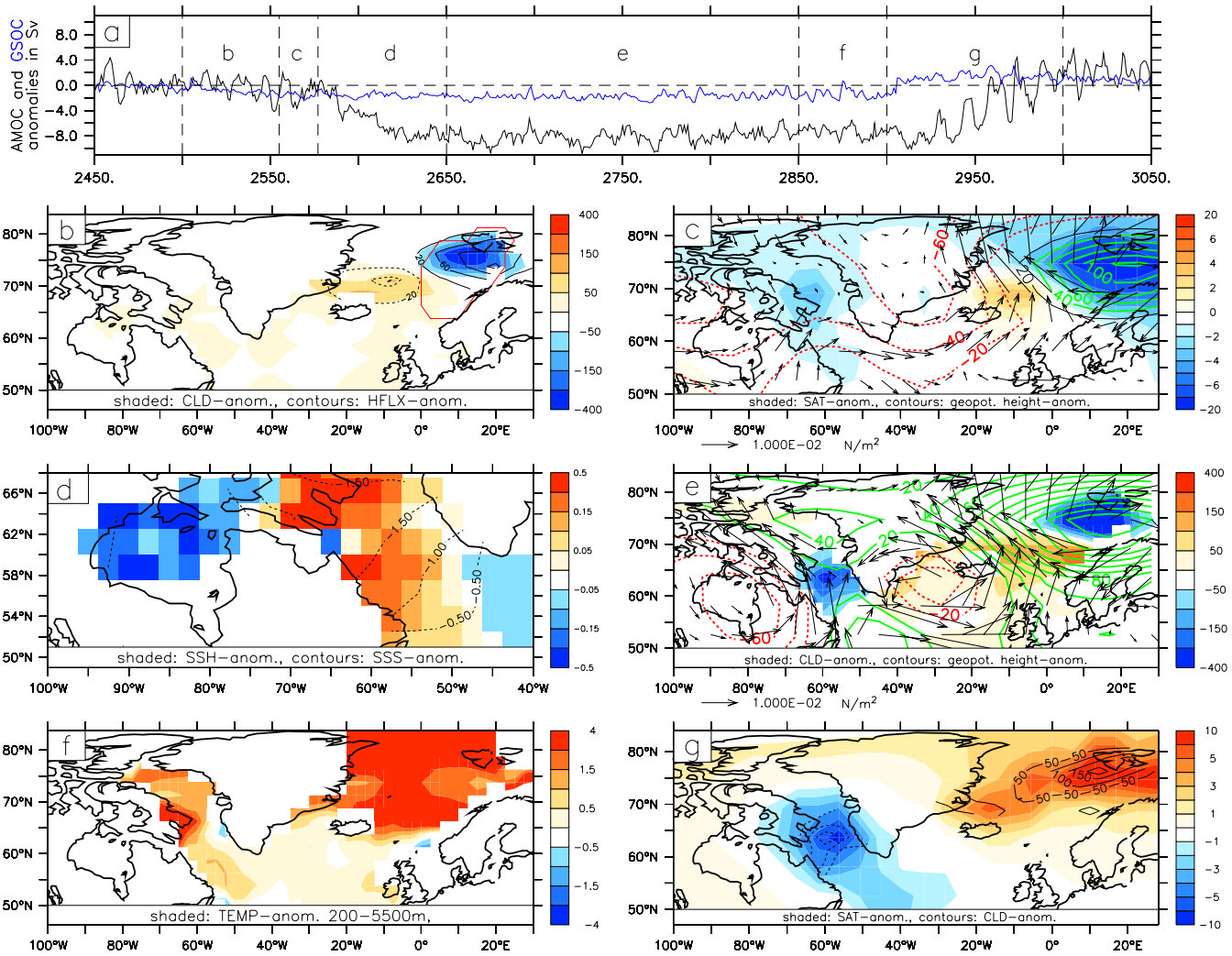

Fig. 3. **(a)** Anomalies of AMOC (black) and GSOC (blue) in Sv for the OBL22.4 run for the timeframe 2450–3050 (see also Fig. 2c,h). Dashed vertical lines denote averaging intervals for panels b-g of this figure. **(b)** Anomalies in convective layer depth (CLD) in m (shaded) and surface heat flux (HFLX) in W/m^2 (contours). A positive HFLX anomaly is associated with a lower-than-normal heat loss of the surface ocean to the atmosphere. The red line indicates the mean GIN Sea sinking region in the model. **(c)** Anomalies of surface air temperature (SAT) in K (shaded), 800 mbar geopotential height in m^2/s^2 (contours) and surface wind stress in N/m^2 (arrows). **(d)** Anomalies of sea surface height in m (shaded) and sea surface salinity in psu (contours). **(e)** Anomalies in CLD in m (shaded), 800 mbar geopotential height in m^2/s^2 (contours) and surface wind stress in N/m^2 (arrows). **(f)** Anomalies of oceanic temperature in K averaged over 200–5500 m. **(g)** SAT anomalies in K (shaded) and CLD anomalies in m (contours). All anomalies in panels b-g are calculated against a strong AMOC state (years: 2400–2450) and averaged over the interval indicated by the respective letter in panel a.

is still advected into the Nordic Seas and the Arctic at depths of 500–1500 m. Due to the lack of deep ocean convection, the inflowing warm and salty North Atlantic waters are not mixed with colder surface waters any more. The subsurface temperatures and salinities in the GIN Sea become decoupled from the surface processes. Decomposing the impact of deep decoupling on the vertical density gradient reveals opposing effects of thermal and haline density components. In the absence of mixing with fresher surface water a salinity anomaly of 0.2–0.4 psu forms in depths >800 m. In conjunction with surface salinities being lower by about 2 psu this tends to stabilize the water column. But in the course of an AMOC weakening event the anomalies in vertical temperature gradient outbalance the ones in salinity and the water column becomes unstable. The increase of subsurface heat content eventually reduces the vertical density gradient to a point when surface convection is re-initiated (Fig. 3g). Previously stored subsurface heat is vented to the surface. Sea-ice coverage reduces and surface air temperature increases by up to 10 K. Associated atmospheric circulation changes generate surface wind anomalies near Hudson Bay, a reduction of snow fall in that area and a re-establishment of the

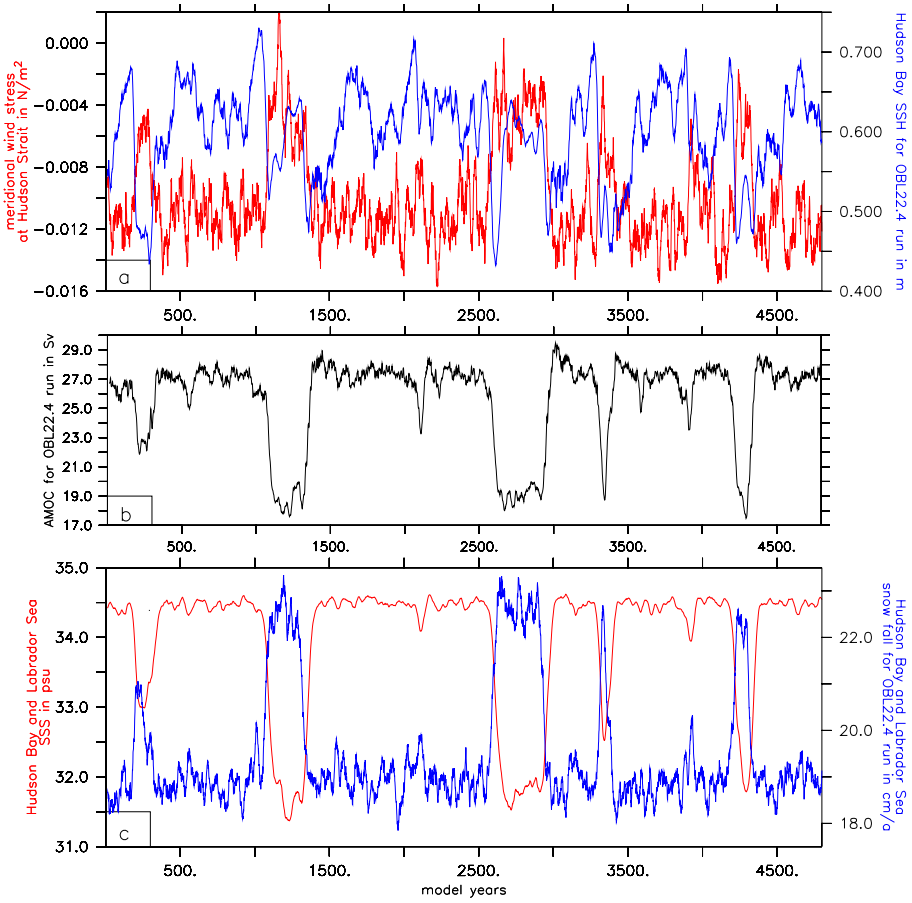

Fig. 4. Timeseries of variables for OBL22.4 run: **(a)** meridional wind stress at Hudson Strait (80° W:70° W, 60° N:70° N) (red) in N/m^2 and Hudson Bay (100° W:75° W, 52° N:70° N) sea surface height in m (blue) for OBL22.4 run. **(b)** AMOC in Sv for OBL22.4 run for comparison. **(c)** SSS in psu (red) and snow fall in cm/a (blue) averaged over Hudson Bay and Labrador Sea (100° W:45° W, 50° N:70° N) for OBL22.4 run in Sv. A running mean of 25 years was applied for all timeseries.

original zonal salinity gradient between the Hudson Bay and the Labrador Sea. These processes initiate the recovery of the AMOC. As stated in the preceding analysis, meridional wind stress at the Hudson Strait as well as snow fall over the Hudson Bay and the Labrador Sea form the key elements for triggering an overturning weakening in the Labrador Sea. Figure 4 shows a timeseries of these variables for the entire OBL22.4 model simulation. It becomes apparent that for all AMOC reductions observed in our simulation a meridional wind stress at the Hudson Strait and an increase in snow fall in this region is in phase with a decreasing AMOC demonstrating that the mechanism described above applies for all individual AMOC events.

A more detailed analysis of the stochastic excitations of the GSOC (not shown) revealed the link between background climate and role of sea ice in amplifying random negative GSOC anomalies. A randomly occurring negative GSOC anomaly reduces poleward heat transport into the sinking regions. The resulting local increase of sea ice depends on the background climate. With lower obliquity values or a higher albedo respectively and hence colder summers there is a greater chance for the sea-ice anomaly to persist into the winter season. This leads to a reduction of air-sea fluxes and eventually an amplification of the negative GSOC anomaly. If these anomalies persist, the resulting atmospheric response (Fig. 3c) can trigger the mechanism described above.

4.3 Sensitivity experiments

To further elucidate what physical processes are responsible for the generation of simulated millennial-scale AMOC variability a series of sensitivity experiments was conducted. A key component of the proposed mechanism (Sect. 4.2) is the large-scale atmospheric response to GIN Sea temperature anomalies, which plays a fundamental role in flushing Hudson Bay freshwater anomalies into the Labrador Sea and hence in weakening the AMOC.

Here, we will address the question whether the simulated atmospheric anomaly pattern (Fig. 3c) is a consequence of the initial GSOC weakening and how it interacts with the latter.

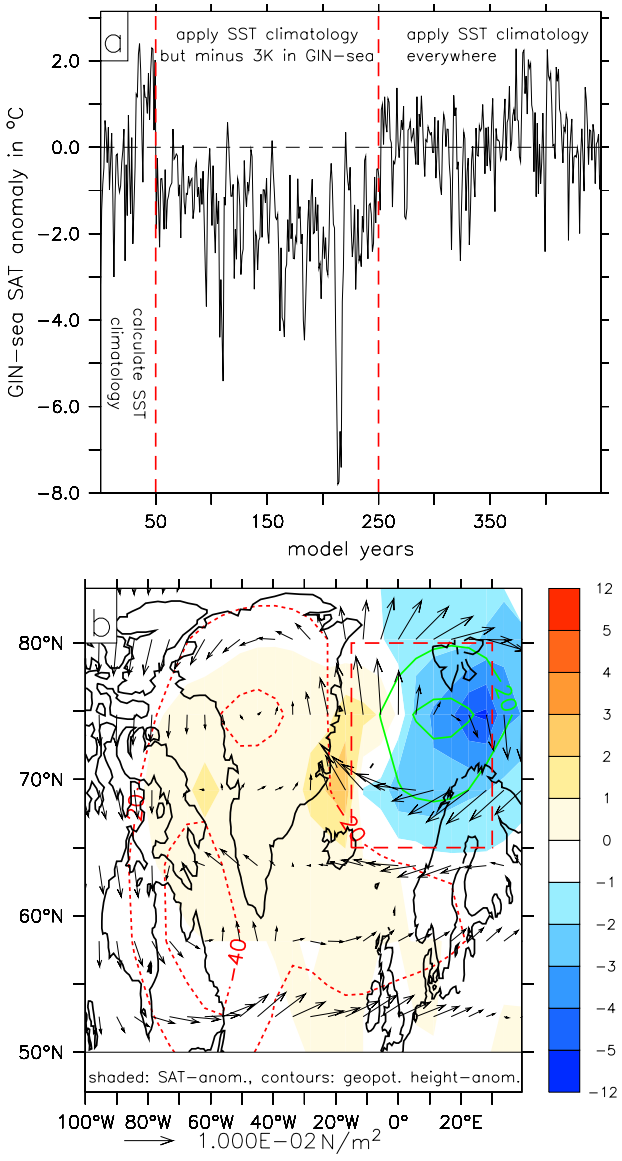

Fig. 5. (a) GIN Sea SAT anomaly (averaged over 15° W to 30° E and 65° N to 80° N) with respect to the model years 1 to 50 of the sensitivity experiment. The red lines separate the three stages of the experiment. **(b)** Anomalies in SAT in K (shaded), 800 mbar geopotential height in m^2/s^2 (contours) and wind stress (arrows) with respect to the model years 1 to 50 of the sensitivity experiment. The red rectangular indicates the region where the SST perturbation is applied to the GIN Sea atmosphere. Please refer to Sect. 4.3 for details.

We repeated the OBL22.4 run starting from a strong AMOC state. In the first 50 model years a sea surface temperature (SST) climatology was generated. Subsequently this climatology was applied for 200 model years everywhere as a lower boundary condition for the atmospheric model, except for the GIN Sea, where simulated temperatures were lowered artificially by lowering SST (as seen by the atmospheric model) year-round by an additional 3 K (see Fig. 5b). Thereafter, climatological SST forcing was applied for another 200 model years. Figure 5 shows the SAT, 800 mbar geopotential height and surface wind stress response to the GIN Sea SST perturbation. Anomalous high pressure forms in the eastern GIN Sea in response to the lower-than-normal SST. Low pressure anomalies develop over Greenland and east of the Hudson Bay, in good qualitative agreement with the diagnosed atmospheric circulation changes during a weakened GSOC state (Fig. 3c). This experiment supports the notion of a strong atmospheric teleconnection between the GIN Sea and the western North Atlantic that was proposed in Sect. 4.2 to explain the connection between GSOC and AMOC.

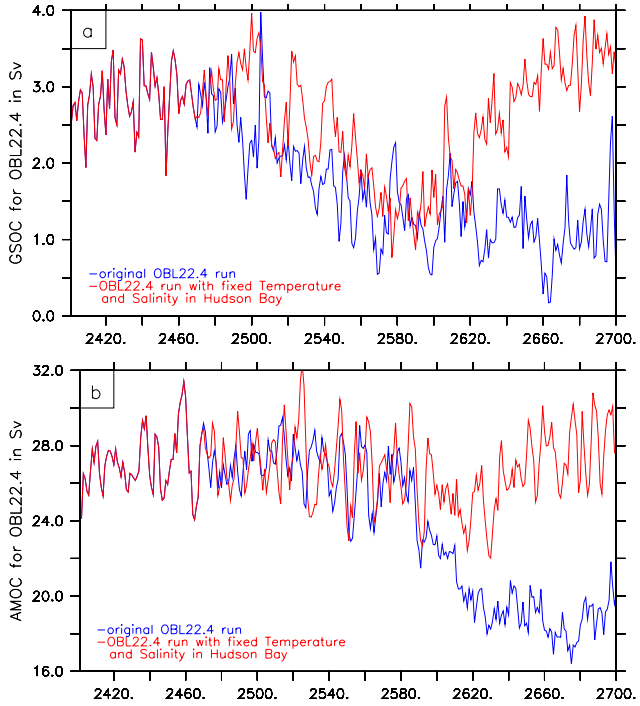

Fig. 6. (a) GSOC for original OBL22.4 run (blue) and (red) a restart of OBL22.4 run in which a temperature and salinity "climatology" in the Hudson Bay was generated from the years 2401 to 2450 and prescribed for 950 model years. **(b)** Same as in (a) for AMOC. Please refer to Sect. 4.3 for details.

In a second sensitivity run we further investigated the role of the Hudson Bay in triggering the observed AMOC oscillations. The OBL22.4 run was repeated starting from model year 2401 during a strong AMOC state (see Figs. 2c, h and 3a). In the first 50 model years temperature and salinity climatology was generated for the Hudson Bay and subsequently applied for 950 years. As can be seen in Fig. 6, the initial GSOC reduction still occurs in the perturbed run. However, due to prescribed salinity and temperature in the Hudson Bay a fresh water pulse is suppressed and the teleconnection between GIN sea and Labrador Sea described above cannot be established. Thus the GSOC reduction does not trigger a convection shut-down in the Labrador Sea.

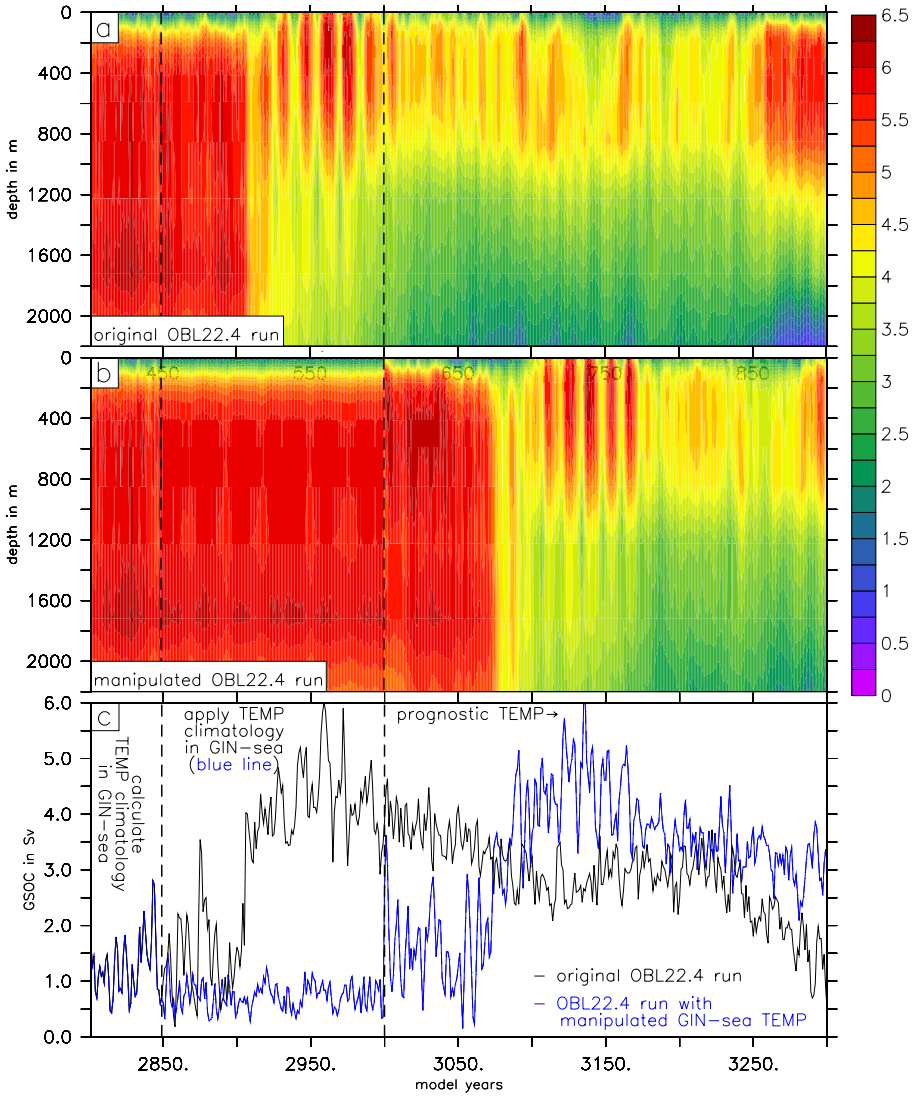

Fig. 7. Hovmoeller diagrams of temperature averaged over GIN Sea in °C for original OBL22.4 run **(a)** and **(b)** a restart of OBL22.4 run in which a subsurface temperature "climatology" in the GIN Sea was generated from the years 2801 to 2850 and prescribed for years 2851 to 3000. Subsequently the model were run another 300 years with prognostic temperatures in the GIN Sea. **(c)** GSOC for original (black line) and manipulated (blue line) OBL22.4 run in Sv for timeframe 2801–3300. Please refer to Sect. 4.3 for details.

To demonstrate the effects of subsurface ocean warming on the recovery of the GSOC we designed a fully coupled experiment in which subsurface temperatures between 200–5500 m were climatologically prescribed in the GIN Sea during a weak GSOC phase. In this sensitivity experiment we repeated the OBL22.4 run for 500 years starting in a weak GSOC/AMOC state (year 2801, see Figure 2c,h). Here, the first 50 model years were used to create a subsurface temperature climatology for the GIN Sea. This climatology was then prescribed for the GIN Sea for the subsequent 200 years for water depths between 200–5500 m. The model was integrated for another 300 years with prognostic temperatures everywhere, including the GIN Sea. The resulting GSOC and subsurface temperatures (averaged over the GIN Sea) can be seen in Fig. 7a,b. Shortly after model year 2900 GSOC in the original OBL22.4 (Fig. 7a and black line in c) experiment recovers abruptly. However, in the sensitivity run (Fig. 7b and blue line in c) prescribed subsurface temperatures impede further warming of sub thermocline waters in the GIN Sea. Accordingly stratification is not eroded and GSOC stays in a weak state. After returning to fully prognostic temperatures in the GIN Sea in model year 3001 GSOC increases by about 0.5 Sv and fully recovers in a thermohaline flush around model year 3100. This sensitivity experiment demonstrated that subsurface warming in the GIN Sea, that is reminiscent of deep-decoupling dynamics, plays a key role in the recovery of the AMOC.

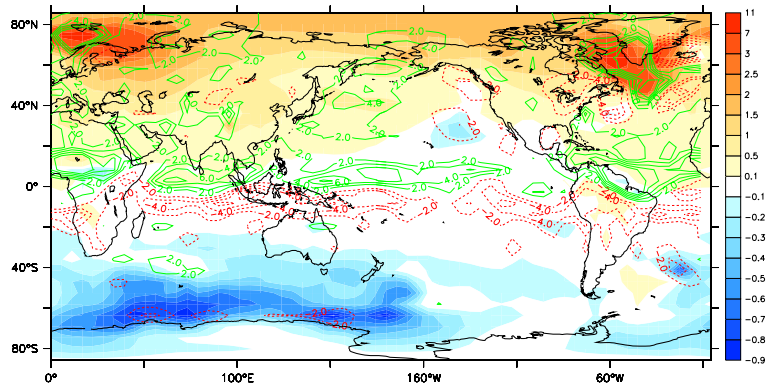

Fig. 8. SAT difference in K (shaded) and precipitation difference in cm/yr (contours) between a strong and a weak AMOC state for the OBL22.1 run. A weak (strong) state is defined by an AMOC <21 Sv (>27 Sv). See also Fig. 2i. Note the non-linear color scale for SAT difference.

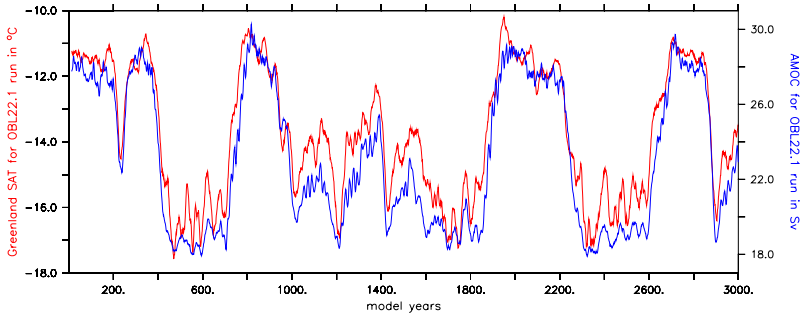

Fig. 9. Red: SAT over Greenland in °C for OBL22.1 run. SAT was averaged over 60° W to 30° W and 60° N to 80° N. Blue: AMOC for OBL22.1 run in Sv. A running mean of 25 years was applied for both timeseries.

4.4 Global impacts of millennial-scale AMOC variability

In our model simulations, the consequences of an abrupt AMOC reduction of about 30% (in the case of the OBL22.4 and OBL22.1 run) can be detected on a global scale. Figure 8 shows the simulated composite differences in SAT and precipitation between a strong (AMOC >27 Sv) and a weak (AMOC <21 Sv) AMOC state for the OBL22.1 experiment. The main response pattern is the so-called bi-polar seesaw (Broecker, 1998) with large-scale warming in the Northern Hemisphere and cooling in the Southern Hemisphere. This pattern is associated with a northward displacement of the Intertropical Convergence Zone for strong overturning in the North Atlantic (Fig. 8). Over Greenland, millennial-scale SAT anomalies attain magnitudes of up to 7 K and are closely linked with ±6 Sv AMOC variations (Fig. 9). Simulated millennial-scale surface air temperature variations as well as their corresponding hydrological effects resemble the spatio-temporal characteristics of the well-known DO oscillations (Dansgaard et al., 1982; Stott et al., 2002; EPICA Community Members, 2006; Tjallingii et al., 2008). The simulated warming over Antarctica during the weak AMOC state accounts for ∼50% of the increase in SAT estimated by EPICA Community Members (2006).

Whereas the simulated rainfall anomalies are relatively small (5–10%) over the equatorial oceans, their relative magnitudes over the Sahara and the Sahel are very considerable (∼40%). The precipitation and temperature changes induce variations in terrestrial vegetation. Periods characterized by a weak AMOC are associated with a reduced terrestrial carbon stock (Fig. 10a,b). On the other hand, the relatively cold conditions prevailing during weak AMOC periods lead to greater CO_2 solubility and an increased storage of carbon in the ocean. During a weak AMOC state, the decrease in terrestrial vegetation is not entirely balanced by increased CO_2 solubility. Hence weak AMOC states are accompanied by an overall increase of atmospheric CO_2 by about 6 ppm. A similar mechanism for externally forced millennial-scale CO_2 variations was already proposed in Menviel et al. (2008). However, it was already noted in Menviel et al. (2008) that the details of the terrestrial and marine carbon cycle response to AMOC variations may strongly depend on the climate background state. Under colder and drier glacial conditions, the terrestrial carbon response might be reduced significantly.

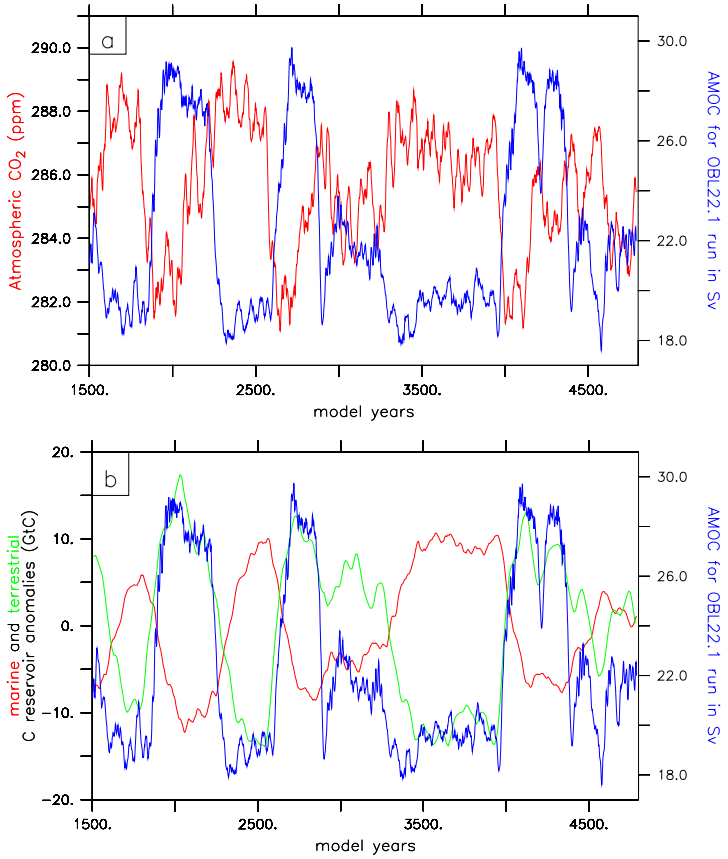

Fig. 10. (a) Atmospheric CO_2 content (red) in ppm and AMOC (blue) for OBL22.1 run. **(b)** Carbon reservoir anomalies for the ocean (red) and the vegetation (green) in GtC and AMOC (blue) for OBL22.1 run in Sv. A running mean of 25 years was applied for all timeseries.

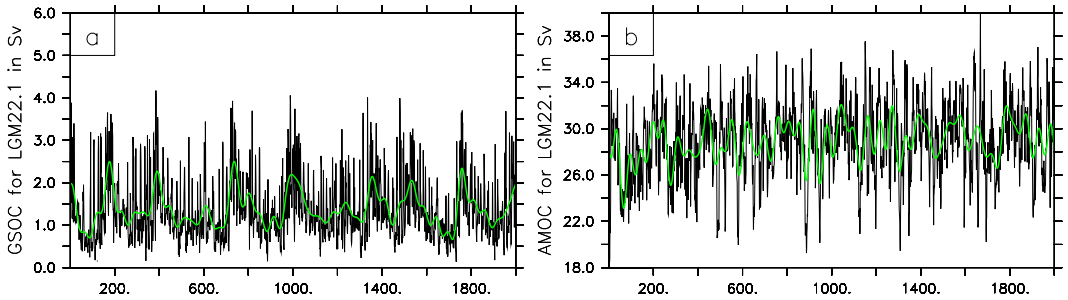

Fig. 11. GSOC **(a)** and AMOC **(b)** in Sv for an obliquity of 22.1 but LGM-bathymetry. A low pass filter of 50 years was applied for green lines.

4.5 Effects of LGM bathymetry

The driving mechanism for centennial-to-millennial-scale AMOC variability in our model heavily relies on the emergence of freshwater flushes from the Hudson Bay into the Labrador Sea and the subsequent reduction of Labrador Sea convection. However, during the last glacial period Hudson Bay was covered by the Laurentide ice sheet. Thus we expect that LGM boundary conditions would prevent the generation of low-frequency AMOC variability in the LOVECLIM model. To demonstrate this effect we repeated the OBL22.1 run using an estimate of the LGM-ocean bathymetry (LGM22.1 run, Table 2) (Roche et al., 2007). In addition, the river runoff mask as well as the land-sea fraction mask were adjusted to LGM values. Atmospheric topographic forcing was kept at present-day values.

Figure 11 clearly shows that LGM-bathymetry suppresses millennial-scale AMOC variability. Even though the GSOC index exhibits some sawtooth behaviour with multiple, rapid increases of ∼1.5 Sv followed by gradual reductions, no

significant centennial-to-millennial scale variability can be seen for the AMOC. A more detailed analysis (not shown) revealed that the atmospheric response to GSOC reductions is similar to the one shown in Fig. 3c with anomalous high-pressure over the GIN Sea sinking region and lower pressure between the southern tip of Greenland and Iceland. However, in the absence of a "freshwater pool" such as the Hudson Bay this atmospheric teleconnection is not able to trigger changes of Labrador Sea convection and hence suppresses AMOC variability.

5 Conclusions

This paper explored the mechanism responsible for the generation of centennial-to-millennial scale AMOC oscillations in the LOVECLIM climate model. Our findings show that these nonlinear and stochastically excited oscillations disappear under glacial boundary conditions (namely glacial bathymetry). Similar to the findings presented by Schulz et al. (2007) we conclude that the mechanism identified for our model solution must be fundamentally different from the one that triggered real Dansgaard-Oeschger events during the last glacial period.

We also conducted several experiments with boundary conditions intermediate between pre-industrial and LGM as described in Rial and Yang (2007) and Rial and Saha (2008). We were able to reproduce their modelling results qualitatively using flat ice-sheet boundary conditions and different orbital configurations. Hence, we assume that the physical mechanism underlying the millennial-scale DO-like oscillation in Rial and Yang (2007) and Rial and Saha (2008) is the same as the one diagnosed in our study. However, our closed Hudson Bay experiments and the sensitivity experiment using prescribed salinity in the Hudson Bay clearly demonstrate that the mechanism that is powering the simulated centennial-millennial-scale oscillations in ECBilt-CLIO/LOVECLIM has to be distinct from the one that triggers Dansgaard-Oeschger oscillations in reality – in contrast to the conclusions of Rial and Yang (2007) and Rial and Saha (2008).

The oscillations identified in ECBilt-CLIO described in Schulz et al. (2007) and Jongma et al. (2007) share several important features with the millennial-scale oscillations in our study. Among them are the atmospheric anomaly pattern, the magnitude of the AMOC oscillations and the important role of salinity. However, there appear to be key differences in the model simulations, such as the lack of a convection breakdown in the GIN Sea in Schulz et al. (2007). Furthermore, their advective horizontal recovery mechanism for Labrador Sea convection contrasts our deep-decoupling resumption mechanism for the GIN Sea.

While the oscillatory model solution may depend strongly on regional features, such as the existence or absence of the Hudson Bay, the overall simulated teleconnection patterns bear quite some similarity to those observed for DO events. In accordance with numerous paleo-data, we found that the ± 6 Sv variations of the AMOC are accompanied by the bipolar seesaw pattern in surface air temperature and large-scale changes of tropical hydroclimate, with the northern tropics drying and the southern tropics becoming wetter for weak overturning in the North Atlantic. Corresponding precipitation changes affect the overall terrestrial carbon stock and hence atmospheric CO_2. A +6 Sv (-6 Sv) change of the AMOC generates atmospheric CO_2 anomalies of of -3 ppm (+3 ppm). Future higher resolution ice-core data from Antarctica might help to confirm whether DO events were in fact accompanied by significant CO_2 variations in the direction predicted here.

Our coupled modelling results lend further support to the concept of deep-decoupling oscillations in 3-D coupled climate models. Identified previously in simplified climate models (Ganopolski and Rahmstorf, 2002; Timmermann et al., 2003) or idealized OGCMs (Winton and Sarachik, 1993), our more realistic model configuration demonstrated the possibility for the emergence of deep-decoupling phases in the GIN Sea. By preventing deep-ocean warming in the GIN Sea we were able to suppress the rapid recovery of the AMOC.

Acknowledgements. T. Friedrich and L. Menviel are supported by the National Science Foundation under grant number ATM-0712690. A. Timmermann and O. Timm are supported by the Japan Agency for Marine-Earth Science and Technology (JAMSTEC) through its sponsorship of the International Pacific Research Center. D. M. Roche is supported by NWO under the RAPID project ORMEN. We thank Andrey Ganopolski and an anonymous reviewer for their constructive and helpful comments that helped to improve the manuscript. This is IPRC number 710 and SOEST contribution number 7974.

Edited by: M. Kawamiya

References

Aeberhardt, M., Blatter, M., and Stocker, T. F.: Variability on the century timescale and regime changes in a stochastically forced zonally averaged ocean-atmosphere model, Geophys. Res. Lett., 27(9), 1303-1306, doi:10.1029/1999GL011103, 2000.

Alley, R. B., Anandakrishnan, S., and Jung, P.: Stochastic Resonance in the North Atlantic, Paleoceanography, 16, 190–198, 2001.

Broecker, W. S.: Paleocean circulation during the last deglaciation: A bipolar seesaw?, Paleoceanography, 13, 119–121, 1998.

Broecker, W. S., Bond, G., and Klas, M.: A salt oscillator in the glacial Atlantic? 1. The concept, Paleoceanography, 5, 469–477, 1990.

Brovkin, V., Ganopolski, A., and Svirezhev, Y.: A continuous climate-vegetation classification for use in climate-biosphere studies, Ecol. Model., 101, 251–261, 1997.

Dansgaard, W.: Evidence for general instability of past climate from a 250 kyr ice-core records, Nature, 364, 218–220, 1993.

Dansgaard, W., .Clausen, H., Gundestrup, N., Hammer, C. U., Johnsen, S. F., Kristinsdottir, P. M., and Reeh, N.: A new Greenland deep ice core, Science, 218, 1273–1277, 1982.

Deser, C., Magnusdottir, G., Saravanan, R., and Phillips, A.: The effects of North Atlantic SST and sea-ice anomalies on the winter circulation in CCM3, Part II: Direct and indirect components of the response, J. Climate, 17, 877–889, 2004.

Driesschaert, E.: Climate change over the next millennia using LOVECLIM, a new Earth system model including the polar ice sheets, Ph.D. thesis, Université Catholique de Louvain, Louvain-la-Neuve, Belgium, available at: http://dial.academielouvain.be: 8080/vital/access/services/Download/boreal:5375/PDF_01 (last access: 17 August 2010), 2005.

EPICA Community Members: One-to-one coupling of glacial climate variability in Greenland and Antarctica, Nature, 444, 195–198, 2006.

Ganopolski, A. and Rahmstorf, S.: Rapid changes of glacial climate simulated in a coupled climate model, Nature, 409, 153–158, 2001.

Ganopolski, A. and Rahmstorf, S.: Abrupt glacial climate change due to stochastic resonance, Phys. Rev. Lett., 88, 0385011–0385014, 2002.

Goosse, H., Deleersnijder, E., Fichefet, T., and England, M.: Sensitivity of a global coupled ocean-sea ice model to the parameterization of vertical mixing, J. Geophys. Res., 104(C6), 13681–13695, 1999.

Goosse, H., Renssen, H., Selten, F. M., Haarsma, R. J., and Opsteegh, J. D.: Potential causes of abrupt climate events: A numerical study with a three-dimensional model, Geophys. Res. Lett., 29(18), 1860, doi:10.1029/2002GL014993, 2002.

GRIP Project Members: Climate instability during the last interglacial period recorded in the GRIP ice core, Nature, 364, 203–207, 1993.

Johnsen, S. J., Clausen, H. B., Dansgaard, W., Gundestrup, K. F. N., Hammer, C. U., Iversen, P., Jouzel, J., Stauffer, B., and steffensen, J. P.: Irregular glacial interstadials recorded in a new Greenland ice core, Nature, 359, 311–313, 1992.

Jongma, J. I., Prange, M., Renssen, H., and Schulz, M.: Amplification of Holocene multicentennial climate forcing by mode transitions in North Atlantic overturning circulation, Geophys. Res. Lett., L15706, 34, doi:10.1029/2007GL030642, 2007.

Levitus, S.: Climatological Atlas of the World Ocean, Tech. rep., NOAA Prof. Paper 13, 1994.

Liu, Z., Otto-Bliesner, B.-L., F. He, E. B., R. Tomas, P. C., Carlson, A., J. Lynch-Stieglitz, W. C., Brook, E., Erickson, D., Jacob, R., Kutzbach, J., and Cheng, J.: Transient Simulation of the Last Deglaciation with a new Mechanism for Bølling-Allerød Warming, Science, 325, 310–314, 2010.

Menviel, L., Timmermann, A., Mouchet, A., and Timm, O.: Meridional reogranization of marine and terrestrial productivity during Heinrich events, Paleoceanography, 23, PA1203, doi:10.1029/2007PA001445, 2008a.

Mouchet, A. and Francois, L. M.: Sensitivity of a global ocean carbon cycle model to the circulation and the fate of organic matter: Preliminary results, Phys. Chem. Earth, 21, 511–516, 1996.

NGRIP Project Members: High-resolution record of Northern Hemisphere climate extending into the last interglacial period, Nature, 431, 147–151, doi:10.1038/nature02805, 2004.

Oeschger, H., Beer, J., Siegenthaler, U., Stauffer, B., Dansgaard, W., and Langway, C.: Late glacial climate history from ice cores, Climate Processes and Climate Sensitivity, 29, 299–306, 1984.

Paul, A. and Schulz, M.: Holocene climate variability on centennial-to-millennial time scales: 2. Internal feedbacks and external forcings as possible causes, in: Climate development and history of the North Atlantic Realm, edited by: Wefer, G., Berger, W. H., Behre, K.-E., and Jansen, E., Springer-Verlag, Berlin, 55–73, 2002.

Pikovsky, A. S. and Kurths, J.: Coherence resonance in a noise-driven excitable system, Phys.l Rev. Lett., 78, 775-778, doi:10.1103/PhysRevLett.78.775, 1997.

Rial, J. and Saha, R.: Stochastic Resonance, Frequency modulation and the Mechanisms of Abrupt Climate Change in the Arctic, First International Symposium on Arctic Research, Drastic Change Under Global Warming (ext. abs.), Miraikan, Tokyo, 94–97, 2008.

Rial, J. A. and Yang, M.: Is the frequency of abrupt climate change modulated by the orbital insolation?, edited by: Hemming, S., Geophysical Monograph Series, Washington, DC, 173, 167–174, 2007.

Roche, D. M., Dokken, T. M., Goosse, H., Renssen, H., and Weber, S. L.: Climate of the Last Glacial Maximum: sensitivity studies and model-data comparison with the LOVECLIM coupled model, Clim. Past, 3, 205–224, doi:10.5194/cp-3-205-2007, 2007.

Schulz, M., Paul, A., and Timmermann, A.: Relaxation oscillators in concert: A framework for climate change at millennial timescales during the late Pleistocene, Geophys. Res. Lett., 29(24), 2193, doi:10.1029/2002GL016144.

Schulz, M., Prange, M., and Klocker, A.: Low-frequency oscillations of the Atlantic Ocean meridional overturning circulation in a coupled climate model, Clim. Past, 3, 97–107, doi:10.5194/cp-3-97-2007, 2007.

Stocker, T.: The seesaw effect, Science, 282, 61–62, 1998

Stommel, H.: Thermohaline convection with two stable regimes of flow, Tellus, 13, 224–230, 1961.

Stott, L., Poulsen, C., Lund, S., and Thuell, R.: Super ENSO and Global Climate Oscillations at Millenial Time Scales, Science, 297, 222–226, 2002.

Timmermann, A. and Goosse, H.: Is the wind-stress forcing essential for the meridional overturning circulation?, Geophys. Res. Lett., 31, L04303, doi:10.1029/2003GL018777, 2004.

Timmermann, A., Gildor, H., Schulz, M., and Tziperman, E.: Coherent resonant millennial-scale climate oscillations triggered by massive meltwater pulses, J. Climate, 16(15), 2569–2585, 2003.

Tjallingii, R., Claussen, M., Stuut, J.-B., Fohlmeister, J., Jahn, A., Bickert, T., Lamy, F., and Röhl, U.: Coherent high- and low-latitude forcing of the Northwest African humidity, Nat. Geoscience, 289, 670–675 doi:10.1038/ngeo289, 2008.

Winton, M.: Deep decoupling oscillation of the oceanic thermohaline circulation, in: Ice in the Climate System, edited by: Peltier, W. R., Springer-Verlag, Berlin, 417–432, 1993.

Winton, M. and Sarachik, E. S.: Thermohaline oscillations induced by strong steady salinity forcing of ocean general circulation models, J. Phys. Oceanogr., 23, 1389–1410, 1993.